Case Studies in Thermal Engineering 68 (2025) 105899

Contents lists available at ScienceDirect

Case Studies in Thermal Engineering

journal homepage: www.elsevier.com/locate/csite

Numerical thermal analysis of a real-case ladle in secondary steelmaking

M. Neri *, H. Soltanian, A.M. Lezzi

University of Brescia, Department of Mechanical and Industrial Engineering, via Branze 38, Brescia, 25103, Italy

HIGHLIGHTS

- The model analyzes the secondary steel-making and the ladle.
- The process dynamic is modeled through 17 sequential time-dependent simulations.
- The power demand decreases over cycles, stabilizing at 1.95 MW/m^3 after six cycles.
- The first cycle demands the most power, consuming 20% of the total.
- The ladle inner temperature drops by 300 °C in 30 min in the first waiting phase, and by 400 °C in 55 min between two production cycles.

ARTICLE INFO

Keywords:
Ladle
Steel-making process
Experimental campaign
Numerical model
Energy demand

ABSTRACT

This paper proposes a 2D axis-symmetric numerical model designed in COMSOL Multiphysics to estimate power demand along the secondary steelmaking process. The analyzed process has been divided into cycles and phases included ladle preheating, waiting, filling, heating, continuous casting, and cleaning. Each cycle is modeled through 17 sequential time-dependent numerical simulations, and has been validated by comparing calculated temperatures with those measured in a steel plant. The study observes that the volumetric power demand decreases progressively over the cycles, stabilizing at 1.95 MW/m^3 after six cycles. Notably, the first cycle is by far the most power-consuming, accounting for nearly 20% of the total. Additionally, the ladle's inner temperature drops by 300 °C within 30 min during the waiting phase between preheating and tapping, and by 400 °C within 55 min between two production cycles. The model is designed to qualitatively evaluate various factors associated with the secondary steel-making process, and it could be used within the framework of a DOE analysis for examining the impact of different variables to optimize energy management and other operations involving ladles.

1. Introduction

The steel-making process is highly energy-intensive and primarily occurs within a ladle, a component designed to hold liquid steel, whose characteristics together with the process conditions influence the energy consumption along the process. The ladle undergoes repeated heating and cooling cycles which make the process unsteady and complex to analyze.

The process comprises several phases and, although the specific production stages may differ based on the type of manufactured steel, there are phases shared across all production processes. As illustrated in Fig. 1, before the beginning of the production cycle, the ladle undergoes several hours of preheating by means of gas burners to minimize thermal shocks from contact with molten steel,

* Corresponding author.
E-mail addresses: manuela.neri@unibs.it (M. Neri), hossein.soltanian@unibs.it (H. Soltanian), adriano.lezzi@unibs.it (A.M. Lezzi).

https://doi.org/10.1016/j.csite.2025.105899
Received 7 August 2024; Received in revised form 10 January 2025; Accepted 15 February 2025
Available online 25 February 2025

Nomenclature

μ	Dynamic viscosity (Pa s)
ρ	Density (kg/m^3)
σ	Stephan Boltzman constant (W/(m^2 K^4))
ε	Emissivity –
k	Thermal conductivity (W/m K)
q'''	Volumetric power (MW/m^3)
F1	Preheating phase
$F1_{bis}$	Initial waiting phase
F2	Tapping phase
F3	Refining phase
F4	Waiting phase
F5	Continuous casting phase
F6	Final waiting phase
amb	Ambient
C	Cycle
c_p	Specific heat (J/kg K)
CC	Continuous casting
E	Energy (kJ)
EAF	Electric arc furnace
f	Final
GCI	Grid Convergence Index
h	Convective heat transfer coefficient (W/m^2 K)
i	initial
L	Characteristic lenght (m)
LF	Ladle furnace
q	Heat flux (W)
Ra	Rayleigh number
S	Surface
S2E	Surface to environment
S2S	Surface to surface
surf	Surface
T	Temperature (K)
t	Time (s)
V	Volume (m^3)
VOD	Vacuum oxygen decarburizing

thereby protecting the refractory materials from potential damage. In the Electric Arc Furnace (EAF), iron scrap and additives placed in a tiltable vessel are melted using electrodes. During the tapping phase, the molten steel is poured into the preheated ladle along with slag, which helps limit heat loss from the steel surface and ensures better temperature control. At this point, the stirring - a process involving blowing argon through a porous plug at the bottom of the ladle - is initiated to homogenize the steel temperature and remove impurities; however, this agitation increases heat loss to the surroundings. Next, the ladle is transferred to the Ladle Furnace (LF), where ferroalloys are added to achieve the desired steel composition, and electrodes immersed in the liquid steel provide energy to reach a threshold temperature. Since the LF is the final phase where the steel temperature can be controlled, the energy input must counteract the cooling effects of adding cold ferroalloys, endothermic reactions, and heat loss. At the end of the process in the LF, to minimize temperature drops, the ladle is covered with a lid. Then, depending on the specific requirements, the ladle can be sent to either the Vacuum Oxygen Decarburizing (VOD) facility or directly to the Continuous Casting (CC) stage. The VOD facility is used for producing high-quality steel by eliminating impurities and enhancing steel quality through the introduction of oxygen. In the CC, molten steel is transformed into final products through the teeming process, where liquid steel is poured into molds via an opening at the bottom of the ladle. Finally, the ladle is taken to a cleaning station to remove residuals of steel and slag. Besides these phases, it is essential to account for holding or waiting periods between each phase, during which the steel temperature gradually decreases, impacting the overall energy demand. The sequence described above, from the preheating to the cleaning of the ladle, represents a cycle.

As described above, except for the melting phase in the EAF, most of the production phases occur within a ladle, a vessel lined internally with refractory bricks resistant to wear processes. As illustrated in Fig. 2, the top part features a slag lining that is highly

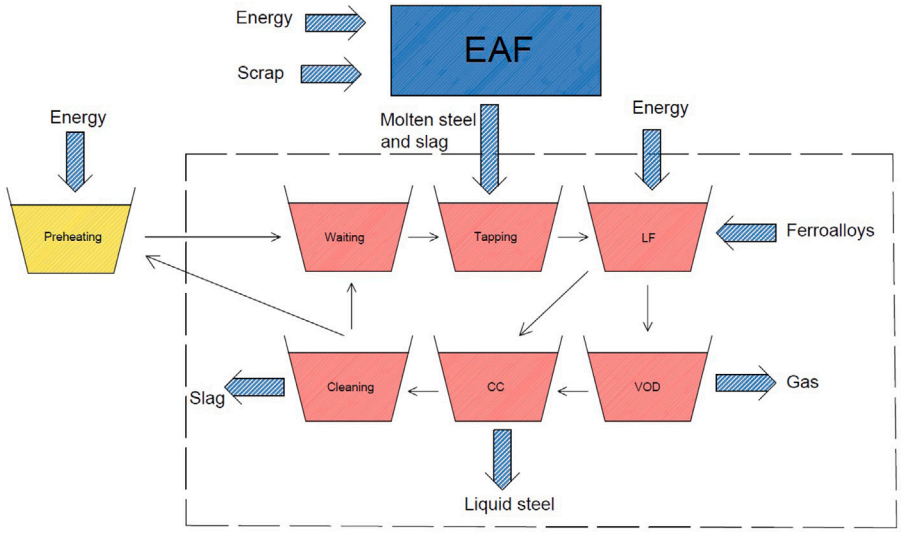

Fig. 1. Representation of the secondary steel-making process. The steps within the dashed box take place in the ladle, which is moved between different processing areas. The preheating phase occurs exclusively during the initial cycle C1, while the VOD process is intended for special steels.

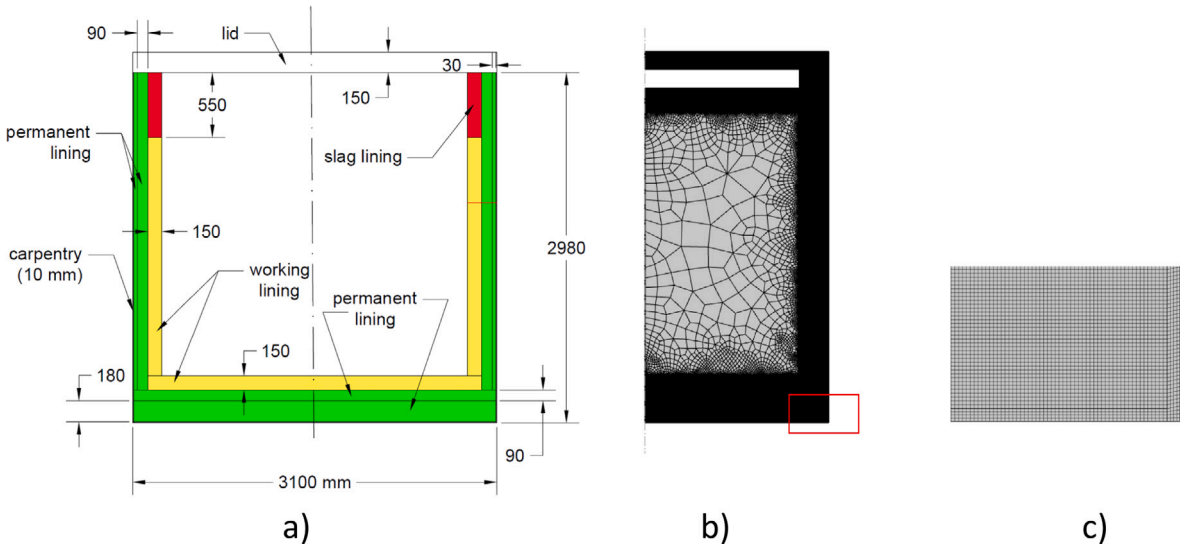

Fig. 2. Ladle geometry (a) and mesh (b,c) defined in the numerical model. The horizontal red line in (a) represents the position where the temperature along the wall thickness has been detected. The mesh is made of square elements of 3 mm throughout the domain, except for the steel domain which, does not necessitate a specialized mesh configuration. Regarding the mesh quality: the average skewness is 0.999, with a minimum of 0.875, the average volume-to-length ratio is 0.999, and the minimum is 0.968, and the growth rate has an average of 1, with a minimum of 0.945. (For interpretation of the references to color in this figure legend, the reader is referred to the web version of this article.)

resistant to corrosion and remains in contact with the slag for most of the time. The walls and base consist of an external steel shell, an intermediate permanent lining, and an internal working lining. The permanent lining protects the steel shell in case of a failure in the innermost layer, maintaining a consistent thickness over time. Since the material of the working lining is critical, as it significantly impacts the ladle's durability, steel manufacturing companies are keenly interested in both its mechanical and thermal performance. A ladle undergoes multiple cycles, during which the thickness of the working lining gradually decreases, with a typical lifespan of 70 to 90 cycles (depending on process conditions) before the refractory requires replacement.

Researches have long been interested in energy efficiency within the metallurgical sector [1–4], and, for the secondary steel-making process, several studies have examined energy consumption across various phases, including the waiting phase [5–7], the tapping phase [8], the stirring and teeming phases [9–11], and the preheating phase [12]. Additionally, some research has focused on the mechanical properties of the ladle [13]. The preheating phase was examined using a 3D combustion and fluid-solid heat transfer model, revealing that covering the empty ladle reduced the steel temperature drop [14]. A numerical study was carried

out to evaluate air temperature and velocity fields in the ladle during the preheating phase, showing that insulation thickness significantly influences temperature distribution, while the distance between the flame and the ladle bottom and the lid-to-ladle distance had only a minor effect [12]. Heat losses through the ladle surface during preheating and the waiting phase, with and without steel were investigated by means of an axial-symmetric modeling [5]. The temperature distribution in the ladle refractory material was experimentally investigated, highlighting the importance of the contact resistance between different layers [6]. In [15], a finite element modeling (FEM) and the Boltzmann mathematical model were used to study the impact of a silica aerogel composite insulation panel installed between the refractory lining and the carpentry, finding that this layer reduces the steel temperature drop by 16 °C. Recent analysis introduced a 1D mathematical model to predict the thermal state of a steel-making ladle, achieving a temperature accuracy within 5 °C for process control and demonstrating sufficient speed for online applications [16]. The impact of slag thickness on heat losses during the waiting phase was numerically assessed considering natural convection in the turbulent regime for liquid steel with the k-ϵ turbulence model. This aspect was numerically evaluated also in [10] employing SIMPLE algorithm, highlighting that thicker slag led to noticable temperature stratification. The effect of stirring on heat losses was examined utilizing a CFD model that included slag, liquid steel, and argon [11]: losses from the free steel surface were considered by comparing three radiation models, namely P-1, discrete-ordinates, and Rosseland. It also evaluated the influence of different ladle materials, slag compositions, and thicknesses. The tapping phase was analyzed using a 2D axisymmetric simulation and experimental data, indicating that refractory material properties have a greater impact on heat losses than thickness [8]. 3D models were used to assess thermal stratification and fluid dynamics during the waiting period, comparing stationary and stirring-induced fluid conditions [9], and to study heat transfer during stirring in the ladle, incorporating molten steel, slag, air, and refractory materials [17]. It was found that a top-free surface with slag and air phases resulted in higher and more uniform temperatures compared to a flat surface without slag. Simulation of the holding period revealed that temperature distribution affects thermal stratification and heat flux, with natural convection creating distinct ricirculation patterns as temperature gradients diminish [18]. A model was proposed to predict coil temperature evolution during the whole thermal cycle process of ladle with a novel steel teeming technology [19]. The study in [20] demonstrated that increasing talc content in periclase-forsterite refractories for steel ladle permanent layers improves thermal insulation by reducing density and thermal conductivity, while increasing porosity. The energy demand throughout the production cycle was numerically estimated in [21], covering stages such as tapping, casting, and preheating.

Steel manufacturing companies aim to reduce energy consumption in their production processes, which is influenced by several factors that cannot be quantified easily at the production site but can be evaluated numerically and by means of the Design Of Experiments (DOE) technique. For instance, it would be useful to assess how different materials in the ladle's layers affect energy consumption. Additionally, the impact of varying the slag thickness could be evaluated, or the influence of a cover during certain phases (where it is currently not used) could be examined. For this kind of analysis, where the effect of a factor on the response is examined, detailed numerical modeling can be impractical since it requires substantial computational resources while companies need results that are both reliable and delivered in a timely manner.

This paper presents a 2D numerical model designed to estimate energy demand in the steel-making process, addressing all key phases experienced by the ladle and accounting for the transient nature of the process. The objective of the model is to serve as a robust tool for reliably and qualitatively estimating the energy demand in the secondary steel-making process, facilitating the comparison of performance across different cycles and refractory materials. The model's computational efficiency has been enhanced through strategic assumptions and simplifications, while its reliability has been verified using experimental data from a production plant, demonstrating both accuracy and practicality. The paper is structured as follows. Section 2 outlines the methods, explains how the secondary steel-making process has been schematized and simulated, and the validation procedures. Section 3 presents and discusses numerical and experimental results concerning temperature distribution on the ladle surface and through the ladle wall thickness. Here, the energy demand estimated along a process performed with a specific ladle is also discussed. Finally, the conclusions summarize the findings and their implications for enhancing energy efficiency in steel-making processes.

2. Methods

This paper proposes a numerical model in COMSOL Multiphysics for evaluating the factors affecting the energy demand in the secondary steel-making process, and by considering all the phases the ladle undergoes to account for the transient nature of the process. The purpose of the model is not to precisely replicate what happens in a steel-making plant, but rather to provide a tool for comparing different scenarios. The model takes into account the progressive emptying of the ladle, an aspect that distinguishes the present study from others in the literature.

The study has been developed in several phases. Initially, it has been necessary to identify a standard production cycle representative of the ladle process: for example, considering the typical operations a ladle undergoes. Moreover, the process in the EAF has been excluded since the ladle is not involved at this stage. Since the model aims to represent most real-world processes for producing non-special steels, it does not take into account processes like VOD. Then, for each phase, geometry and boundary conditions have been determined based on data in the literature, and information provided by a steel plant. To limit computational effort, conduction, convection, and radiation phenomena have been considered but the enhancement of energy transport due to vigorous molten steel flow has been accounted for by imposing a uniform time dependent temperature distribution. This eliminates the need of solving the Navier–Stokes equations reducing the complexity of the model definition and the computational time; this makes the model suitable also for steel-making companies interested in qualitative data for comparison. Next, to validate the model, temperature data obtained from a production plant for both the molten steel and the ladle surface have been compared with numerical values. Finally, the initial cycles of steel production have been simulated to evaluate the power demand and the temperature variations of the ladle throughout the process.

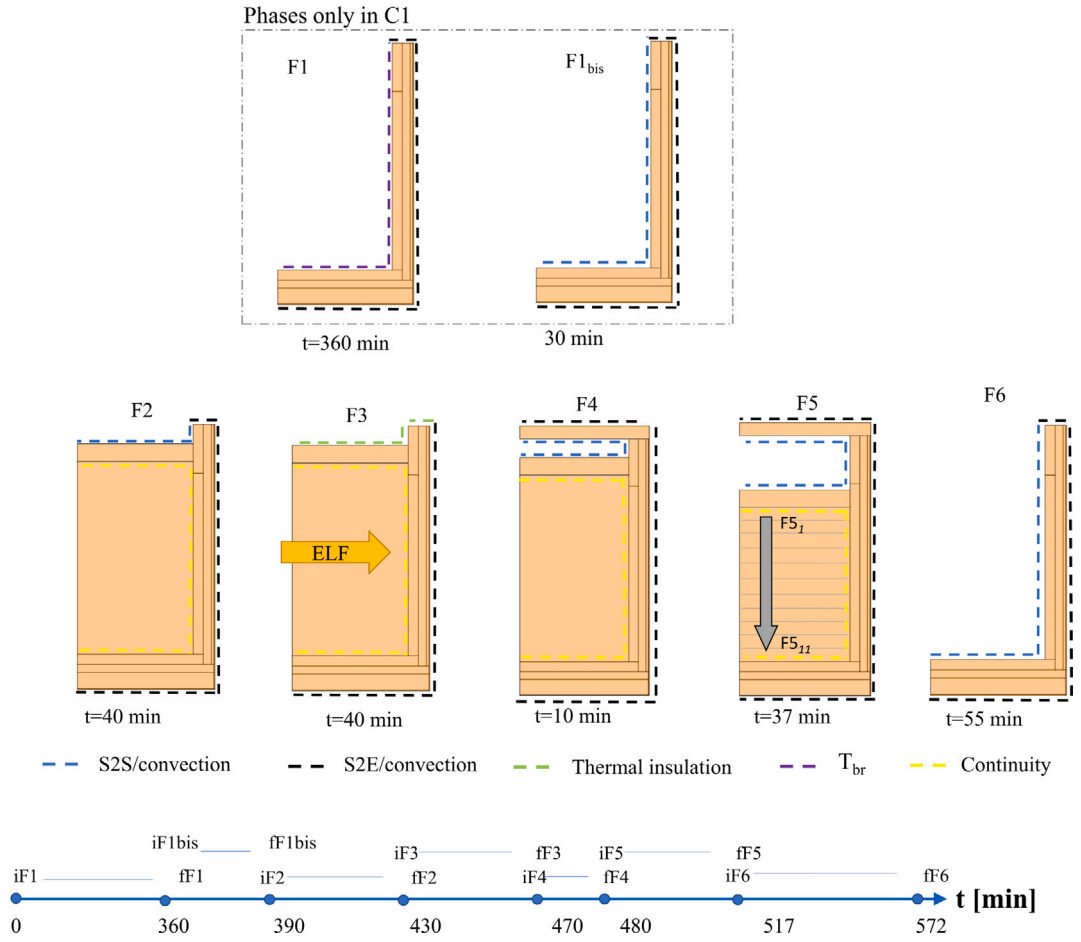

Fig. 3. Schematization of the production cycle and boundary conditions defined in the model. The geometry of the model varies according to the phase of the process. The preheating phase (F1) and the initial waiting phase ($F1_{bis}$) take place only during the first cycle (C1). For the teeming phase (phase F5), which involves the emptying of the ladle, the process has been simulated through a series of 11 numerical sub-simulations.

2.1. Schematization of the secondary-steel making process

Real steel production process can vary significantly due to factors such as steel quality and production demands, which affects also the process duration. This study proposes a numerical model based on standardized phases sequences and time duration obtained from both in the literature and a steel production facility. The modeled process is schematized as a sequence of cycles (C) and phases (F); each phase represents a distinct process that the ladle undergoes, while a cycle comprises all the phases. The phases considered are the following. The preheating (F1) and the subsequent initial waiting ($F1_{bis}$) are applicable only to the first cycle (C1). The other phases occur in all cycles and they are tapping phase (F2) in which the ladle is filled with molten steel, refining treatment in the LF (F3), waiting (F4), teeming (F5), that is, the emptying in the CC facility, and final waiting (F6) during which the ladle is cleaned. The preheating (F1) is performed only when the ladle initially enters the production process; thereafter, the ladle arriving from the CC remains sufficiently hot to avoid thermal shock to the working lining. Fig. 3 depicts the various phases, geometry, and timing: the letters *i* and *f* denote the start and end times of each phase, respectively. For example, C1_F2_f indicates the final time of phase F2 in the first cycle. Each phase is simulated numerically, and F5 involves 11 sub-simulations to accommodate variations in the liquid steel level. Thus, a cycle comprises all the phases required to convert a specified amount of scrap into the finished product, including additional phases for ladle cleaning.

2.2. Numerical model

In this section, the numerical model defined for investigating the energy demand in the secondary steel-making process is presented. To simulate a cycle, the model involves 15 numerical simulations (except for C1 which involves 17 simulations) and each of them uses the temperature distribution achieved in the proceeding simulation as its initial condition. The geometry varies between simulations as shown in Fig. 3. The model accounts for a time-dependent study where two physics have been considered,

Table 1
Materials properties set in the numerical model. The properties without references were obtained from catalogs provided by refractory material manufacturers.

Material	ρ [kg/m^3]	k [W/m K]	c_p [J/kg K]	ε [–]
Lid	2390	1.35	1000	0.45 [23]
Slag	2800 [11]	0.48 [11]	520 [11]	0.6
Permanent lining wall	2700	2.2 [13]	1047	–
Permanent lining bottom	2100 [24]	2 [24]	1047 [24]	–
Carpentry	7200 [11]	52 [11]	787 [11]	0.9 [8]
Liquid steel	6981 [25]	41 [25]	783 [25]	–
Magnesia	3030	8 (0 °C) 6 (400 °C) 4.8 (800 °C) 4 (1200) [26]	1300 [27]	0.45
Slag lining	3030	8 (0 °C) 6 (400 °C) 4.8 (800 °C) 4 (1200) [26]	890 (200 °C) 1060 (700 °C) 1144 (1200 °C) [5]	0.8 [5]

that is, the heat transfer in solid since convection in the liquid steel is not simulated (as explained in the following), and the radiative heat transfer (both to ambient, and surface-to-surface (S2S) [22]). The S2S heat transfer model uses the ray shooting algorithm to model radiative heat transfer, and heat flux at each boundary element on the surface is computed by sending rays outward from the surface to query the temperatures of other surfaces in the geometry. The implicit solver type and the BDF method have been selected. The initial time step is specified as 0.001 min, after which the software dynamically adjusts the time step, with a maximum step size of 0.1 min since only conduction is solved.

2.2.1. Model geometry and materials

As explained above, the ladle goes through several phases, each characterized by different conditions: sometimes it contains steel, other times it is closed with a lid, and boundary conditions vary accordingly. Whether the steel in the ladle may be present or not, the geometry of the ladle does not change along the process and it is shown in Fig. 2. The ladle's wall and base include three layers: an internal working lining, a safety lining, and an external carpentry. Different geometries have been identified for the distinct phases, as schematized in Fig. 3. In the preheating (F1), initial waiting ($F1_{bis}$), and final waiting (F6) phases, the ladle is empty and not covered, while the presence of a lid has been considered in the waiting (F4) and teeming (F5) phases. During the tapping (F2), refining (F3), waiting (F4) and teeming (F5) phases, the ladle contains both steel and slag. As detailed below, to ensure the reliability of the results regardless of grid dimensions, a sensitivity analysis has been performed, and the results have led to a domain discretized with square elements of 3 mm, except in the steel domain, where an unstructured grid is used due to the boundary condition defined. Each of the phases shown in Fig. 3 has been analyzed through one or more numerical simulations: to take into account the transitory nature of the process, the temperature distribution computed at the end of each simulation has been used as the initial condition for the following one. This implies that to determine the power demand in a given cycle, all preceding cycles must be simulated because they are interdependent. Table 1 reports the materials properties set in the model, and it can be seen that some of them exhibit temperature-dependent values; the model standardizes the properties of steel, and disregards chemical reactions and compositional variations. Whenever possible, data provided by refractory material manufacturers have been used, although in most cases, the properties have been reported at a single temperature, corresponding to the operating temperature. Since the model is designed to compare the energy demand as a function of the refractory material used in the working lining rather than simulate the operation of a real steel production plant, this simplification does not compromise the validity of the results.

2.2.2. Boundary conditions

In the model, the boundary conditions vary depending on the phase according to Fig. 3. Both convection and radiation phenomena, in addition to conduction, have been considered. On the external surface of the ladle, a surface-to-ambient (S2E) heat transfer model has been applied, while a surface-to-surface (S2S) model has been used on the internal surface [22]. Therefore, the total heat flux q is given by:

$$q = \mathrm{h} \cdot (T_{surf} - T_{amb}) + \sigma \cdot \varepsilon \cdot \left(T_{surf}^4 - T_x^4\right) \tag{1}$$

where h is the convective heat transfer coefficient, and σ is the Stefan–Boltzmann constant, ε is the surface emissivity, T_{surf} is the considered surface temperature, and T_x can be either the temperature of another surface or the ambient temperature, this latter assumed equal to 25 °C.

The governing equations for convection heat transfer coefficient are as follows [5]:

$$h = \frac{k}{L}\left\{0.825 + \frac{0.387\,Ra^{1/6}}{\left[1+\left(\frac{0.492\cdot k}{\mu\cdot c_p}\right)^{9/16}\right]^{8/27}}\right\}^2 \qquad \text{for } Ra > 10^9 \tag{2}$$

for the vertical surfaces of the ladle;

$$h = \frac{k}{L}\left(0.27Ra^{1/4}\right) \qquad \text{for } T_{surf} > T_{amb} \text{ and } 10^5 \le Ra \le 10^{10} \tag{3}$$

$$h = \frac{k}{L}\left(0.15Ra^{1/3}\right) \qquad \text{for } T_{surf} \le T_{amb} \text{ and } 10^7 \le Ra \le 10^{11} \tag{4}$$

for the bottom of the ladle, the slag free surface, and the lid surfaces; where L is the characteristic length of the surface, Ra is the Rayleigh number, k, c_p, and μ are the thermal conductivity, the specific heat capacity, and the viscosity of air, respectively. The software COMSOL Mutliphysics automatically calculates the heat transfer coefficient depending on temperature, surface orientation, and characteristic length of the surface of interest.

Phase-specific boundary conditions

The boundary conditions vary depending on the considered phase, and are presented below. It is reminded that phases F1 and $F1_{bis}$ are only present in the first cycle (C1).

F1 - *Preheating* of the ladle In this phase, crucial for preventing thermal shocks that could damage the refractory lining upon contact with the molten steel, the ladle is heated using gas burners inserted from the top. Although the time duration may vary based on the specific production process, in the model it has been set equal to 15 h to reflect the typical practice of the company providing the experimental results discussed. The effect of the gas burners has been simulated by setting a time-dependent Dirichlet boundary condition on the internal vertical and horizontal surfaces of the ladle (as depicted in Fig. 3), and obtained from experimental data collected in the production plant, as Eq. (5):

$$T_{br} = \begin{cases} 25\ °C + \frac{1100\ °C - 25\ °C}{11h}\cdot t, & \text{if } 0 < t \le 11\,h \\ 1100\ °C, & \text{if } 11\,h < t < 15\,h \end{cases} \tag{5}$$

where t represents time in hours. The curve is characterized by a first phase which involves a ramp-up designed to increase the temperature proportionally, and a second maintenance phase which ensures that heat penetrates even into the deeper regions of the ladle.

$F1_{bis}$ - *Initial waiting* Once the preheating phase is concluded, the gas burners are removed and the ladle waits to be filled. The inner surface exchanges heat through convection with air at 400 °C [5], coupled with a S2S boundary condition.

F2 - *Tapping* phase: filling of the ladle with molten steel Given that tapping is a relatively quick process, the ladle-filling phase is considered instantaneous. The model defines also the domains for steel and slag, with a total steel mass of 8,846 kg at initial temperature of 1600 °C. Since the vigorous mixing caused by the stirring ensures a quite homogeneous temperature distribution in the steel, instead of modeling convection directly, its effects are accounted for by imposing a uniform, time-dependent temperature across the steel domain, maintained through an isothermal condition [28], assumption that does not allow to capture thermal stratification and fine-scale movements. This simplification is based on the fact that the fluid dynamics are heavily influenced by operational conditions, which can vary significantly from case to case, and it enables the analysis of multiple cycles efficiently, even on computers with limited processing power, ensuring relatively rapid evaluation of the phenomena. Since the model is designed to compare the energy demand as a function of different operating conditions, this simplification does not undermine the model overall purpose, and it makes the computing less time-consuming. A temperature continuity condition has been imposed between the ladle and the steel surfaces, to account for the contact between the steel in movement and the ladle surface. Therefore, the steel temperature is a function of time and not of the position, that is, $T_{steel} = T_{steel}(t)$. This condition does not fully represent reality, but it allows for a simplification by disregarding the conditions within the ladle, which can be influenced by various factors such as argon gas flow rates, arrangement types and number of plug, the difference in density between the gas and liquid steel, and the point of injection.

F3 - *Refining*: heating in the LF This phase simulates the process where energy (E_{LF}) is supplied by means of electrodes to the steel. In real processes, to reach a desired temperature at the end of the refining process, the amount of supplied energy E_{LF} varies as a function of several factors such as the amount of injected argon, the heat losses caused by the opening of the slag layer, the amount of ferroalloys added, etc. To decouple the simulations from the specific steel being treated and to streamline the analysis, the amount of energy supplied has been calculated indirectly by defining a threshold steel temperature, equal for each cycles, to be reached by the end of phase F5. This has been simulated by imposing a uniform, constant volumetric power source term q''' determined iteratively; it is applied on the steel and the slag to reach the temperature threshold of 1595 °C on the steel domain at the final instant of 40 min. This temperature reflects typical values observed in real processes, though it may vary depending on production conditions. The energy demand is then calculated as:

$$E_{LF} = q''' \cdot V \cdot t \tag{6}$$

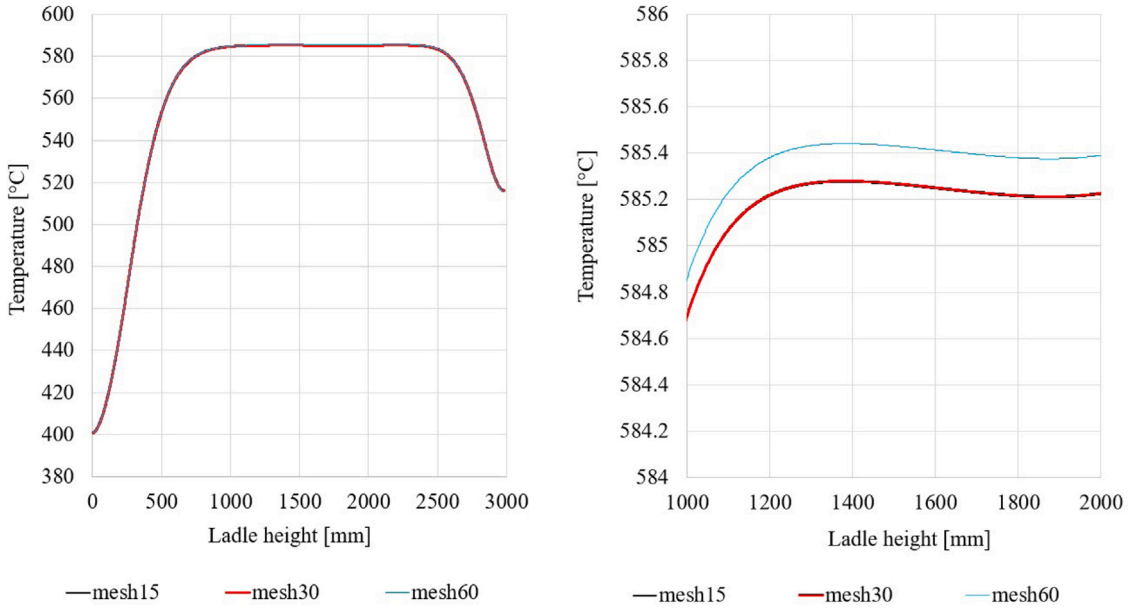

Fig. 4. Comparison of the temperature distribution detected at the end of phase F3 on the external ladle surface for the sensitivity analysis: mesh15 features elements of 1.5 mm, mesh 30 of 3 mm, and mesh 60 of 6 mm.

where V is the volume of steel and t is the time in seconds. Although the study does not directly simulate the irradiation effects from the electrodes on the upper surface of the slag, this influence has been accounted for by applying a thermal insulation condition.

F4 - *Waiting* phase In this phase, the ladle is covered with a lid at an initial temperature of 250 °C, and the temperature of the air between the steel and lid is estimated by the following correlation based on experimental measurements made by the steel-making company:

$$T_{air} = 1.21\ t^3 - 29.58\ t^2 + 249.68\ t + 45.35 \tag{7}$$

where T is in °C and t is measured in minutes.

F5 - *Teeming* phase: emptying of the ladle in CC This phase represents the emptying of the ladle into the continuous casting (CC) system, and it has been analyzed through 11 numerical sub-simulations. In each simulation, the steel level is reduced by 200 mm, and the portion previously occupied by steel is replaced with air at initial temperature of 800 °C. The average temperature of the slag at the end of each simulation is used as the initial condition for the subsequent simulation; since the steel is at a uniform temperature, the final temperature has been applied to the remaining portion in the following simulation.

F6 - *Final waiting* of the empty ladle In this phase, residuals of slag and steel are removed, and the ladle waits to enter the next cycle empty and without the lid. In the model, the ladle is simulated empty, and natural convection and radiation on the ladle surfaces are considered. Also in this case the air in the ladle is considered at 400 °C [5].

2.2.3. Sensitivity analysis and model verification

A sensitivity analysis has been conducted to evaluate the impact of grid cell dimensions; it has been evaluated the temperature distribution across the ladle thickness and the ladle's external surface, and the energy demand E_{LF} estimated in phase *C1_ F3*. Three mesh element sizes have been considered as reported in Table 2. To get an estimate of the value of the energy demand in phase F3 at zero grid spacing, the Richardson extrapolation has been calculated using a safety factor of 1.25, and returns a value of 2.424 MWh/m^3. The grid convergence index GCI is 0.055% when considering mesh15 and mesh30, and 0.442% for mesh30 and mesh60, and this leads to the solutions being in the asymptotic range of convergence. Fig. 4 illustrates the temperature distribution detected for the different meshes across the ladle thickness, while Fig. 5 shows the temperature on the external ladle surface. It can be seen that the temperature trends are very similar. The model is expected to be used for DOE analysis, where computational efficiency is a critical consideration. As such, mesh30 has been identified as the most efficient option for this type of analysis, due to its lower computational time requirements.

To validate the numerical model, an experimental campaign has been conducted at a production facility, where temperatures have been measured on the external surface of a new ladle made of magnesia at various stages of the process. Despite the real process in this analysis included an extended treatment in the LF, the temperature values obtained are still useful for validating the model. Measurements have been taken using an infrared camera THERMO GEAR G120EX, used by the company for control measurements and periodically calibrated in an accredited laboratory. The setting of the camera was adjusted by measuring the

Table 2
Details of the mesh sensitivity analysis. The characteristics of the meshes analyzed for mesh sensitivity are based on a grid refinement ratio of 2. The number of elements corresponds to the geometry in phase F3 and the ladle domain.

Parameter	mesh15	mesh30	mesh60
Dimension of the elements [mm]	1.5	3	6
Number of elements	728 156	182 476	48 341
Time for convergence ($F3$)	39 min	8 min	2 min
E_{LF}	2.423	2.416	2.356

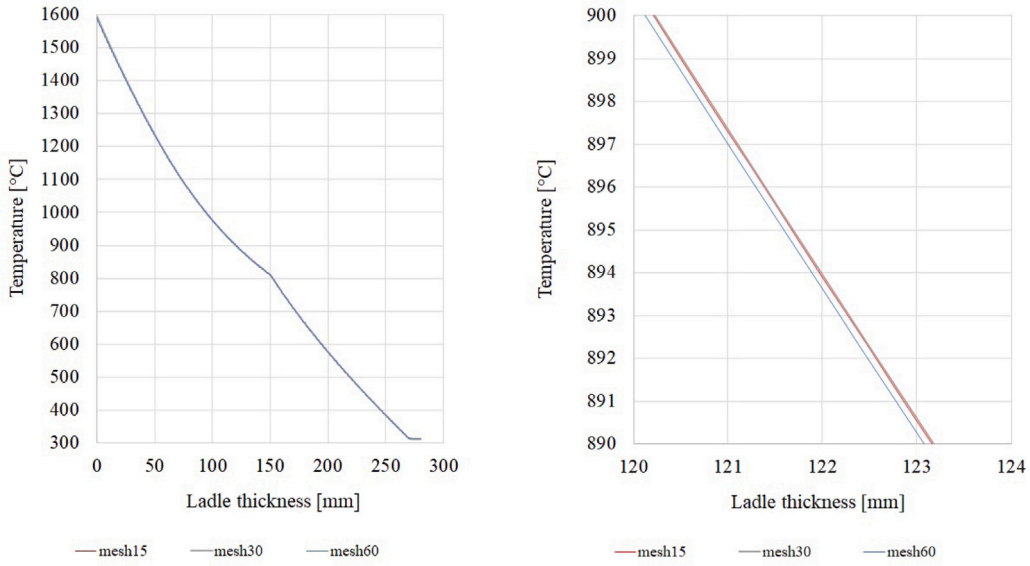

Fig. 5. Comparison of the temperature distribution detected at the end of F3 along the ladle wall thickness (red line in Table 2 a) for the sensitivity analysis: mesh15 features elements of 1.5 mm, mesh 30 of 3 mm, and mesh 60 of 6 mm.

steel temperature and then modifying the emissivity value accordingly. The infrared camera has a measuring range of −40 °C to 1500 °C and an accuracy of ±2 °C. Additionally, the temperature trend of the liquid steel in the teeming phase (F5), which showed a decrease of 0.5 °C per minute, was also considered for validation purposes.

To verify the model's ability to estimate the temperature distribution, values measured at specific points on the outer surface of the ladle have been compared with those predicted by the model. For selected heights, three temperatures have been measured, averaged, and overlaid to the temperature distribution estimated numerically. The graphs in Figs. 6 and 7 indicate that the model is able to reproduce the general trend of the temperatures. The most significant differences were observed during phase F6 (Fig. 7), where the measured temperatures in the upper part of the ladle were significantly higher than those estimated. This phenomenon could be explained by the fact that, in the real process, to allow the removal of slag and residual steel, the ladle is tilted before being put on standby to re-enter the production cycle, exposing the upper part to the heat radiated by the hot residues. The observed discrepancies can be attributed to the increased geometric complexity of the actual ladle compared to the simplified geometry used in the model, as well as the model's inability to fully replicate the actual operating conditions. Despite these differences, the data shows a generally good agreement between the model's estimates and the actual measurements. Fig. 6(d) has been considered to quantify the difference between experimental and numerical outcomes, and a 6.9% relative error shows a reliable validation. The same process is repeated for 6 (b) and 7 (b) offering the relative discrepancy values of 8.3% and 9.2%, respectively.

2.3. Simulations of the first six production cycles

The model has been used to estimate the energy requirements for heating the steel up to 1595 °C by the end of the refining (F3) phase over the first six production cycles. This number of cycles was chosen to approach a steady-state condition, with the energy demand difference between successive cycles being less than 0.5%. The first cycle (C1) includes seven phases (F1-F6), incorporating both the preheating phase (F1) and the initial waiting phase ($F1_{bis}$). Subsequent cycles (C2-C6) consist of six phases (F2-F6). Therefore, a total of 79 numerical simulations have been performed.

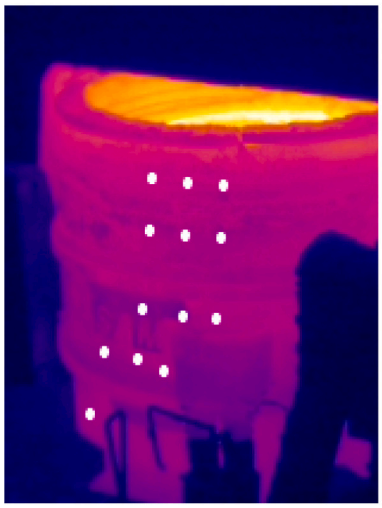

(a)

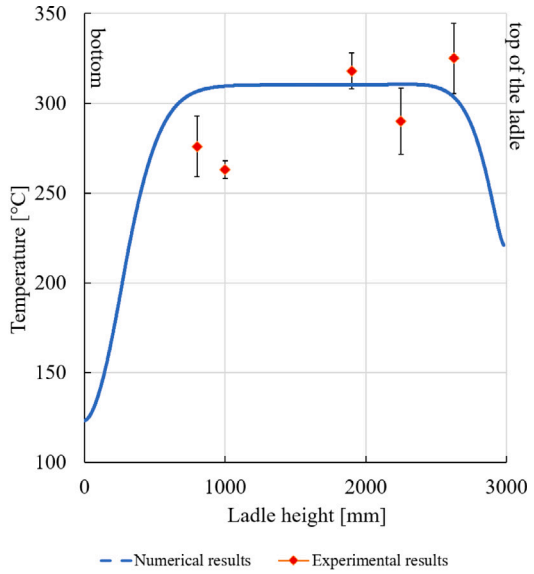

(b)

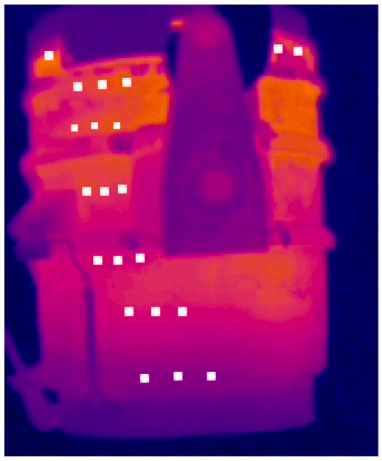

(c)

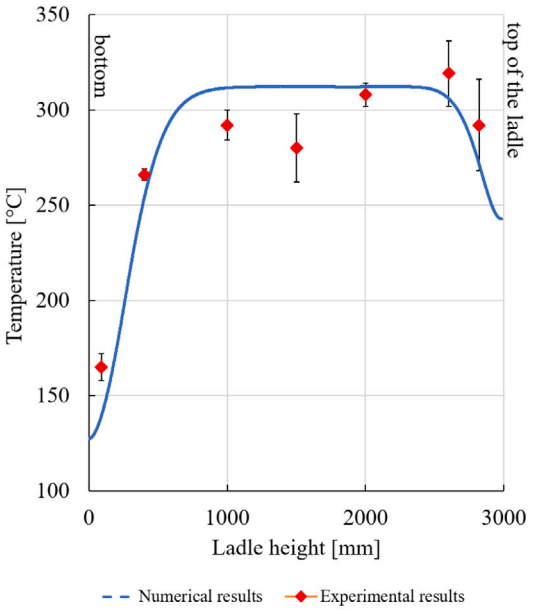

(d)

Fig. 6. Comparison of experimental and estimated data for the final instants of the tapping phase $F2_f$ (**a**, **b**), and the refining $F3_f$ (**c**, **d**) phase. Positions where the temperature has been measured (**a**, **c**). Estimated temperatures compared with those obtained from the thermal imaging (**b**, **d**).

3. Results and discussion

This section presents the findings from an experimental campaign conducted at a production plant, alongside results estimated using the model described in Section 2. The discussion primarily centers on the distribution of temperature within the steel and ladle, as well as the power demand in the LF.

3.1. Comparison of experimental and numerical temperature data

In this section, estimated and measured temperature distribution on the ladle external wall and the temperature trend of the liquid steel have been evaluated to assess whether the model is able to detect the temperature variation along the process.

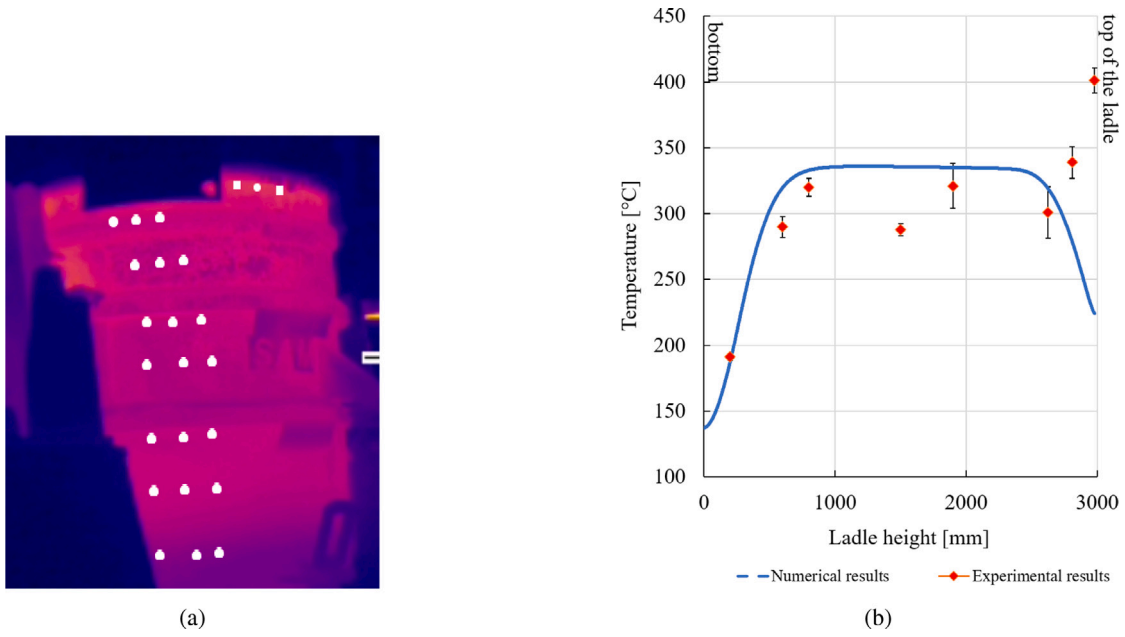

Fig. 7. Comparison of experimental and estimated data for phase $F6_f$: positions of the points where the temperature has been detected (a), and the estimated temperatures compared with those obtained from the thermal imaging (b).

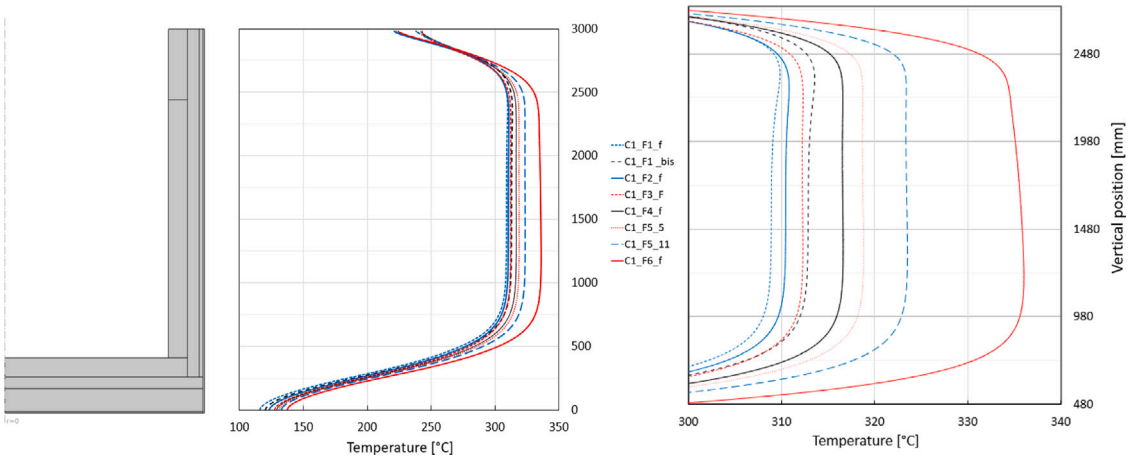

Fig. 8. Temperature distribution estimated on the ladle external vertical surface along the first cycle C1 and magnification of estimated temperatures in the central part of the ladle.

Estimated temperature variation on the ladle surface

Fig. 8 illustrates the temperature distribution estimated on the ladle's external surface at the end of each phase of the first cycle. These values have been compared with those detected in an experimental campaign performed in a production plant and reported in Tables 3–5. Three zones can be recognized: the bottom, the central part, and the top. At the bottom, the temperature does not exceed 300 °C, while at the bottom it is lower than 250 °C, attributable to the thicker insulation layer that separates the surface from the molten steel. Higher temperatures are observed near the top of the ladle, close to the slag lining. The ladle central area, which remains in prolonged contact with molten steel, exhibits the highest temperatures. Here, at the end of the preheating phase ($F1_f$), the temperature is slightly below 310 °C. This temperature rises to approximately 313 °C during the subsequent waiting phase ($F1_{bis}$). During the tapping (F2) phase, despite the molten steel being at around 1600 °C, the ladle wall's high heat capacity causes a slight decrease in the surface temperature to about 311 °C. As in refining (F3) phase energy is supplied to the liquid steel, the external temperature rises reaching approximately 312 °C. This temperature further increases to around 316 °C by the end of the following waiting (F4) phase. During the teeming (F5) phase, which lasts nearly 36 min, the temperature continues to rise, reaching about 323 °C. Finally, by the end of the final waiting (F6) phase, the external temperature exceeds 335 °C.

Table 3
Temperatures detected on the ladle surfaces in the experimental campaign performed in a steel production plant.

A) $F1_{bis}$ TIME 13:44 - After preheating, and before tapping (with empty ladle).

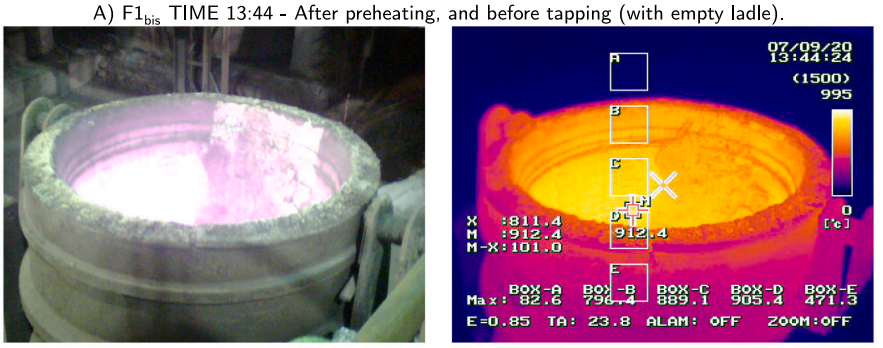

B) $F2_f$ - TIME 13:54 - After tapping before treatment in LF (molten steel in the ladle)

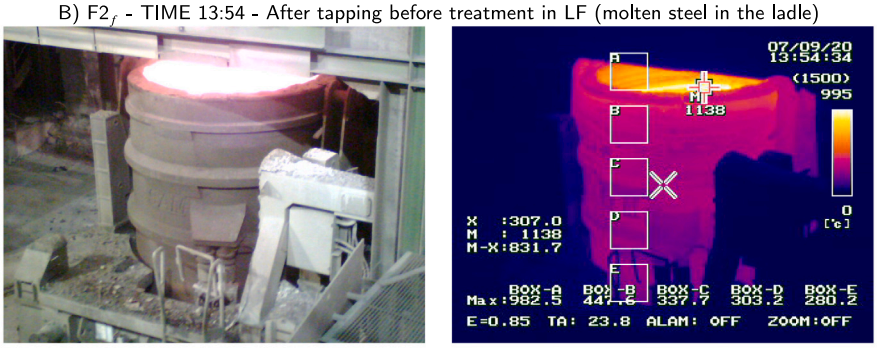

C) $F4_i$ - TIME 15:19 - Ladle covered with lid after LF, ready for continuous casting

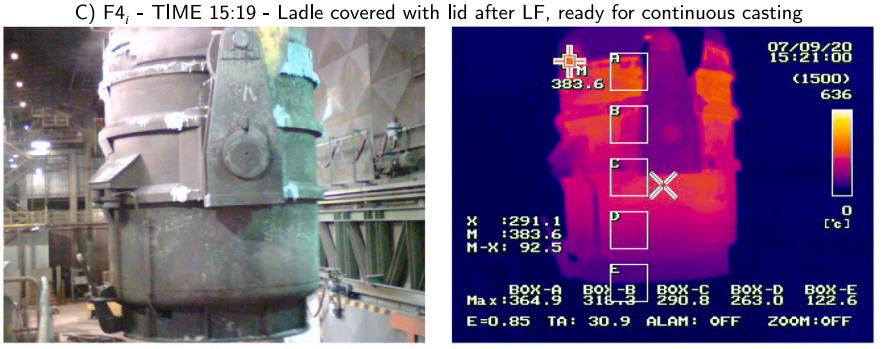

Estimated vs measured temperature

The temperature values discussed above are compared with values in Tables 3–5 detected experimentally in a production plant. According to Table 3, the temperature at the end of initial waiting ($F1_{bis}$) phase varies significantly along the ladle height. Temperatures around 470 °C are observed in the upper section, where the slag lining is located, due to the preheating phase with gas burners, which intensely heat the top portion of the ladle. On the contrary, the boundary conditions set in the numerical model determine a uniform temperature distribution in the order of 220 °C.

Table 3 (b) displays the ladle's temperature upon receiving the liquid steel from the EAF (F2). The highest temperature is recorded at the top of the ladle, and it is in the order of 447 °C, a value lower than the one measured at the end of the preheating (F1) phase. In the tapping (F2) phase the temperature at the center of the ladle is 310 °C, and around 280 °C at the bottom, and results are consistent with the experimental results.

Table 3 (c) presents the ladle after exiting the LF ($F4_i$), after being covered with a lid. Here, the surface temperature decreases by approximately 10 °C, likely due to the ladle being suspended and transported to another facility. The average temperature at the ladle's center remains around 310 °C, while the temperature at the top, near the slag lining, decreases to about 360 °C. Tables 4 (d) and (e) refer to the ladle in the CC utility (F5), and the temperature at the center is around 320 °C, consistent with the temperature of 324 °C estimated numerically.

Table 4 (f) displays the interior of the ladle with residual slag, where the recorded temperature is comparable to the simulation's estimate ($F5_{11}$), which predicts a slag temperature to be 1457 °C. Table 5 (g) reveals that the ladle temperature has increased up to

Table 4
Temperatures detected on the ladle surfaces in the experimental campaign performed in a steel production plant.

D) $F5_5$ - Time:16:05 - Middle point of the treatment in CC. The molten steel is being drained.

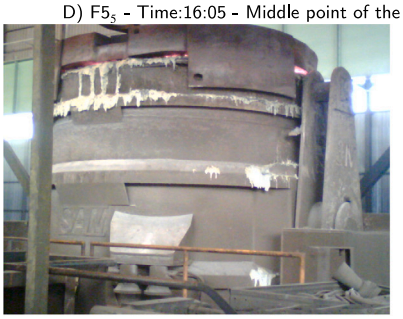

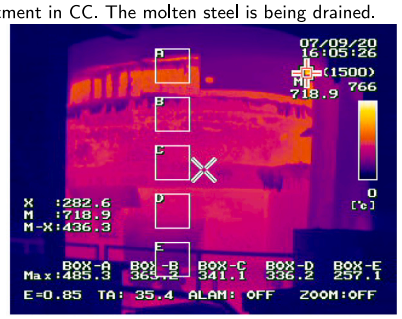

E) $F5_{11}$ - Time: 16:20 - Final point of the treatment in CC. The ladle is empty and removed from the facility.

F) $F6_i$ - Time: 16:32 - Cleaning of the ladle from steel and slag residue.

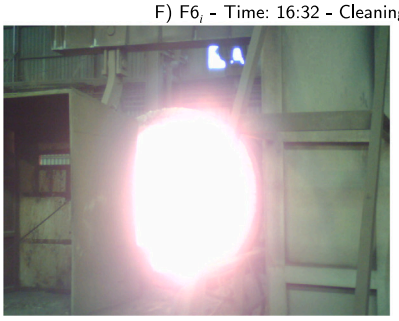

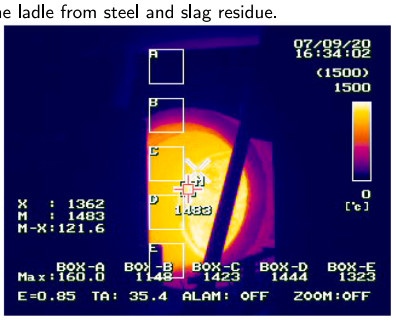

400 °C, due to radiation from the slag beneath the ladle surface. Table 5 (h) indicates that at the end of final waiting (F6) phase, the ladle's external surface temperature reaches 350 °C, which is higher than the value predicted by the model. This discrepancy was expected, given that the real process extended longer than the simulated cycle, leading to higher detected temperatures. Despite this, the model effectively captures the overall trend in temperature variations on the ladle's external surface. Finally, the steel temperature variation of approximately 0.5 °C/min detected at the production plant has been compared with the estimated data in Fig. 9 (a), showing a good agreement.

In light of the findings reported above, it can be stated that the proposed numerical model captures the transient nature of the steel-making process, and it can be used for evaluating different scenarios, especially when analyzing the cause and effect between factors, as well as their combined effects, such as in a DOE analysis.

3.2. Simulation of the production process using a ladle with magnesia lining

The proposed numerical model has been used to simulate the initial six cycles of a production process performed with a ladle made of magnesia, providing energy consumption and temperature distributions across the ladle wall.

Power demand and steel temperature along the production process

The steel temperature trend throughout the first sixth cycles is illustrated in Fig. 9 (a), where it can be seen that the steel temperature decreases during the tapping (F2) phase. This reduction occurs because the steel, initially at 1600 °C, comes into contact with the internal surface of the ladle, which has undergone a pre-heating (F1) followed by a 30-minute waiting period ($F1_{bis}$). During the refining (F3) phase, the steel temperature rises rapidly to 1595 °C due to energy supplied by means of electrodes. In the waiting

Table 5
Temperatures detected on the ladle surfaces in the experimental campaign performed in a steel production plant.

G) F6 - Time: 16:37 - Transportation of the ladle to the final point.

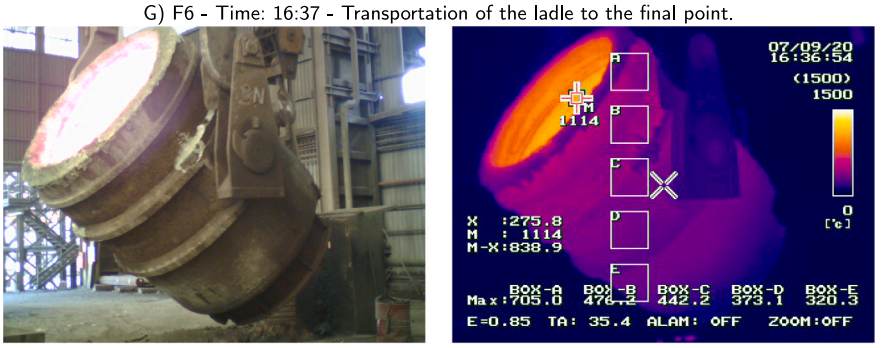

H) $F6_f$ - Time: 16:47 - Finish of the cycle - The ladle is covered and waits to enter the next circle.

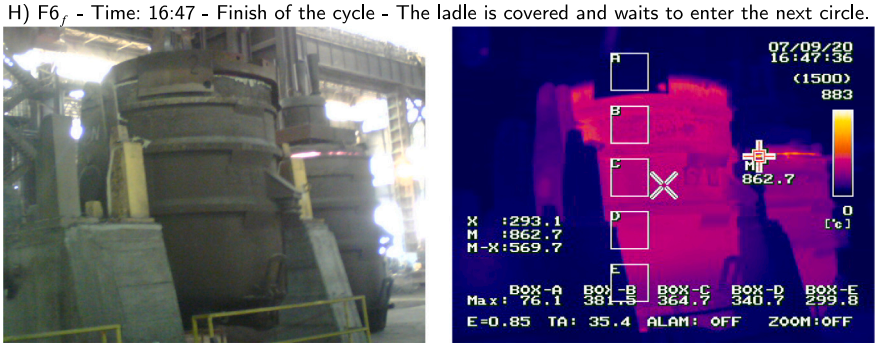

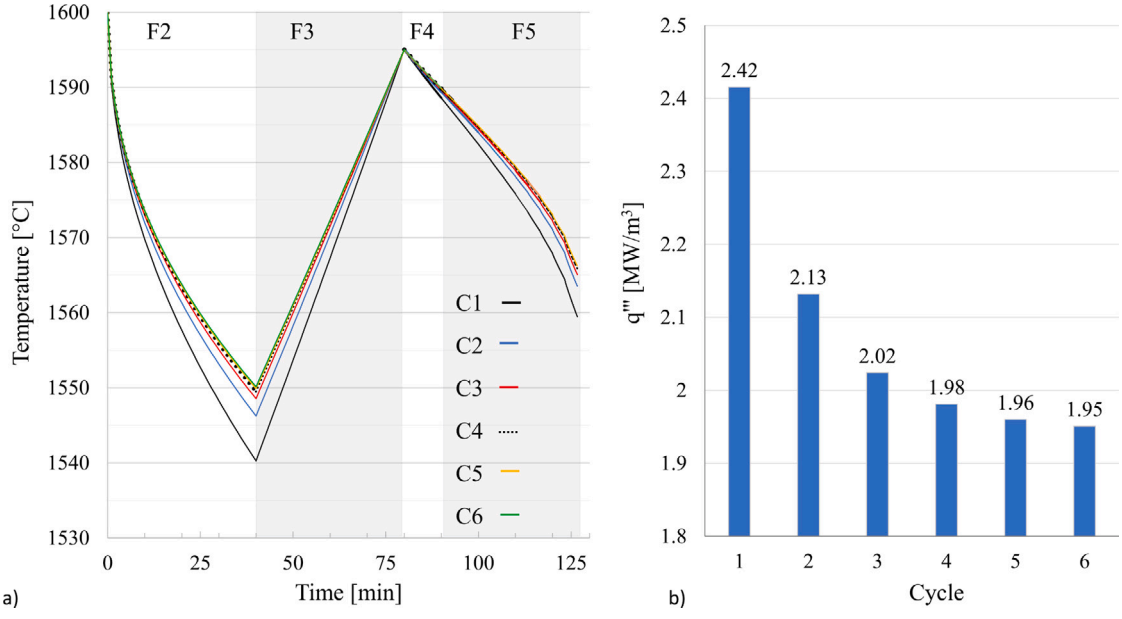

Fig. 9. Numerical results obtained for a ladle with the working lining made of magnesia. Temperature–time trend detected on the steel domain along the first six cycles (a): F2 is representative of the tapping phase when steel is poured into the ladle, F3 of the refining treatment when energy is supplied to the steel, F4 of the waiting phase, and F5 of the teeming phase. Energy demand of the production process across the first six cycles (b).

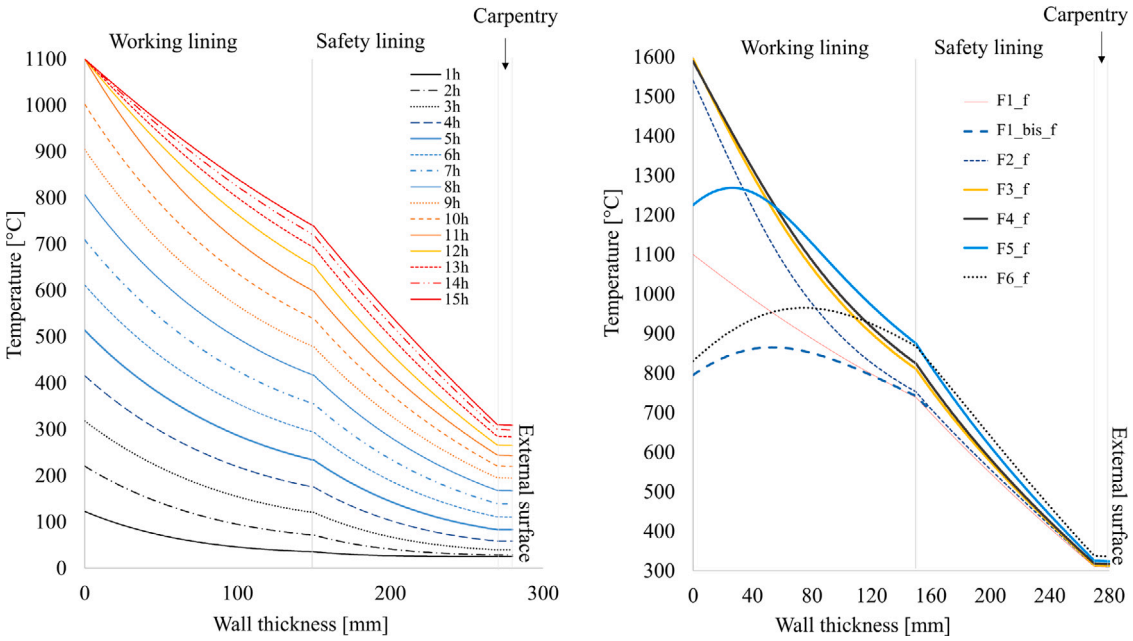

Fig. 10. Temperature detected along the ladle wall thickness on the red line in Fig. 2 along the preheating process $F1$ (a), and at the end of each phase of the first cycle (b).

(F4) and teeming (F5) phases, the temperature decreases more gradually compared to phase initial waiting (F2) phase, attributed to the higher temperature of the ladle. Comparing the temperature trends from cycle C1 to cycle C6, it is evident that the temperature decreases along the cycle is most pronounced in the first cycle, whereas from cycle C3 onwards, the temperature variation becomes less significant.

Fig. 9 (b) illustrates the volumetric power demand q''' over the initial six cycles, representing the power required to achieve a steel temperature of 1595 °C by the end of the refining (F3) phase. The data reveal a decreasing trend in power demand throughout the cycles. By the fifth cycle, the power demand stabilizes at approximately 1.95 MW/m^3, with the variation in power supply between cycles C5 and C6 being less than 0.5%.

Temperature detected in the ladle wall

Temperature detected across the thickness of the ladle at the location indicated by the red line in Fig. 2 are reported in Fig. 10. According to Fig. 10 (a) during the preheating (F1) phase, the temperature rises with a more pronounced increase on the internal surface, and the time duration of this phase is insufficient to achieve a steady condition, as the temperature continues to rise between the fourteenth and fifteenth hours. This trend is likely because the upper limit of T_{br}, set at 1100 °C, is maintained for only 4 h.

At the same position in the wall, the temperature distibution at the end of each phase of cycle C1 is detected and shown in Fig. 10 (b). Two temperature trends are recognizable, one on the internal surface, and the other one in the innermost part of the wall. At the end of the preheating (F1) phase, the temperature on the internal surface is 1100 °C, approximately 400 °C lower than the temperature of the steel arriving from the EAF; temperatures within the working lining range from 1100 °C to 800 °C. During the subsequent waiting ($F1_{bis}$) phase, the temperature on the internal wall drops to approximately 800 °C as a consequence of the exposure to air at 400 °C. In the tapping (F2) phase, the contact with the molten steel raises the inner surface temperature to 1540 °C. The further increase in temperature during the refining (F3) phase is due to the power supplied in the LF. The waiting (F4) phase results in minimal temperature change. By the end of the teeming (F5) phase, the temperature on the inner surface decreases to about 1200 °C, while the innermost part of the working lining still increases in temperature. At the end of the final waiting (F6) phase, the superficial temperature reduces to 800 °C, while the temperature in the safety lining still increases.

Summarizing, it can be stated that the 11-hour preheating period is insufficient to steadly heat the deepest layers of the ladle, which gradually warm up as the production process progresses. Even if the presence of molten steel in the tapping (F2) phase contributes to the temperature rise, the most significant increase occurs during the refining (F3) phase due to the additional energy input. Heat continues to penetrate towards the wall-inner during the teeming (F5) phase, resulting in further temperature elevation. The final waiting (F6) phase causes substantial cooling of the inner surface, although the deepest layers continue to warm. Throughout these phases, temperature variations in the outermost layer remain minimal.

To increase the temperature at the end of the preheating phase (F1), a solution is represented by the use of electric heaters capable of providing preheating up to temperatures of about 1500 °C [29]. To reduce energy consumption, it is advisable to cover the ladle with a lid during the waiting phase ($F1_{bis}$) following preheating, considering that 30 min is a significant interval. Furthermore, closing the ladle after cleaning in phase F6 can further contribute to the reduction of overall energy consumption.

4. Conclusions

The current study presents a 2D axis-symmetric numerical model defined to estimate the power demand along the secondary steel-making process, encompassing ladle preheating, waiting, filling, heating, continuous casting, and cleaning. The entire process has been segmented into cycles and phases, and the cycle dynamics are captured through 17 sequential numerical simulations. The volumetric power demand shows a decreasing trend ranging from 2.42 MW/m^3 and it stabilizes at 1.95 MW/m^3 after 6 cycles. The first cycle is by far the most power-demanding one accounting for 20% of the total power demand. The ladle inner temperature drops by 300 °C in 30 min in the waiting phase between preheating and tapping, and by 400 °C in 55 min in the waiting phase between two production cycles. The energy demand can be reduced by employing electric heaters during the preheating phase and by covering the ladle with a lid after preheating, as the waiting period lasts for 30 min. Additionally, using a lid after ladle cleaning may provide further benefits and warrants investigation. The detailed, phase-by-phase numerical approach provided in this research serves as a valuable tool for comparative analysis and can be applied to other industrial contexts as well. The numerical model is designed to qualitatively analyze various factors related to the secondary steel-making process, with a potential of a DOE analysis where the effects of different factors are examined. While the model does not precisely replicate the conditions within the ladle, certain simplifications make it suitable for extensive simulation campaigns involving numerous cases to be analyzed.

CRediT authorship contribution statement

M. Neri: Writing – review & editing, Validation, Methodology, Investigation, Data curation, Conceptualization. **H. Soltanian:** Writing – review & editing, Writing – original draft, Data curation. **A.M. Lezzi:** Writing – review & editing, Supervision, Project administration, Methodology, Conceptualization.

Declaration of competing interest

The authors declare that they have no known competing financial interests or personal relationships that could have appeared to influence the work reported in this paper.

Data availability

Data will be made available on request.

References

[1] R. Arango-Miranda, R. Hausler, R. Romero-López, M. Glaus, S.P. Ibarra-Zavaleta, An overview of energy and exergy analysis to the industrial sector, a contribution to sustainability, Sustain. 10 (2018) 1–19, http://dx.doi.org/10.3390/su10010153.
[2] K. Wong, Sustainable engineering in the global energy sector, J. Energy Res. Technol. 138 (2015) 024701-024701-4, http://dx.doi.org/10.1115/1.4031783.
[3] A.G. Hernandez, L. Paoli, J. Cullen, Resource efficiency in steelmaking: energy and materials combined, Energy Procedia. 142 (2017) 2429–2434, http://dx.doi.org/10.1016/j.egypro.2017.12.178.
[4] M. Neri, A.M. Lezzi, G.P. Beretta, M.P. Pilotelli, Energy and energy based analysis for reducing energy demand in heat processes for aluminium casting, J. Energy Res. Technol. 141 (2019) 104501, http://dx.doi.org/10.1115/1.4043389.
[5] M.F. Santos, M.H. Moreira, M.G.G. Campos, P.I.B.G.B. Pelissari, R.A. Angélico, E.Y. Sako, S. Sinnema, V.C. Pandolfelli, Enhanced numerical tool to evaluate steel ladle thermal losses, Ceram. Int. 44 (2018) 12831–12840, http://dx.doi.org/10.1016/j.ceramint.2018.04.092.
[6] A. Zimmer, A.N.C. Lima, R.M. Trommer, S.R. Braganca, C.P. Bergmann, Heat transfer in steelmaking ladle, J. Iron Steel Res. Int. 15 (2008) 11–14, http://dx.doi.org/10.1016/S1006-706X(08)60117-X.
[7] J.L. Xia, T. Ahokainen, Transient flow and heat transfer in a steelmaking ladle during the holding period, Met. Mater. Trans. B. 32 (2001) 733–741, http://dx.doi.org/10.1007/s11663-001-0127-2.
[8] B. Glaser, M. Görnerup, D. Sichen, Fluid flow and heat transfer in the ladle during teeming, Steel Res. Int. 82 (2011) 827–835, http://dx.doi.org/10.1002/srin.201000270.
[9] D. Haojian, R. Ying, Z. Lifeng, Fluid flow, thermal stratification, and inclusion motion during holding period in steel ladles, Met. Mater. Trans. B. 50 (2019).
[10] C. Sanjib, S. Yogeshwar, Effect of slag cover on heat loss and liquid steel flow in ladles before and during teeming to a continuous casting tundish, Met. Trans. B. 23 (1992) 135–151, http://dx.doi.org/10.1007/BF02651849.
[11] J.E. Farrera-Buenrostro, C.A. Hernàndez-Bocanegra, J.A. Ramos-Banderas, E. Torres-Alonso, N.M. Lòpez-Granados, M.A. Ramì rez Argàez, Analysis of temperature losses of the liquid steel in a ladle furnace during desulfurization stage, Trans. Indian Inst. Met. 72 (2019) 899–909, http://dx.doi.org/10.1007/s12666-018-1548-9.
[12] B. Glaser, M. Görnerup, D. Sichen, Thermal modelling of the ladle preheating process, Steel Res. Int. 82 (2011) 1425–1434, http://dx.doi.org/10.1002/srin.201100198.
[13] H. Aidong, J. Shengli, H. Harald, G. Dietmar, A method for steel ladle lining optimization applying thermomechanical modelling and Taguchi approaches, J. Min. Met. Mater. 70 (2018) 2449–2456, http://dx.doi.org/10.1007/s11837-018-3063-1.
[14] H. Zhang, P. Zhou, F. Yuan, Effects of ladle lid or online preheating on heat preservation of ladle linings and temperature drop of molten steel, Energy 214 (2021) 118896, http://dx.doi.org/10.1016/j.energy.2020.118896.
[15] L. Zhang, L. Zhu, C. Zhang, Z. Wang, P. Xiao, Z. Liu, Physical experiment and numerical simulation on thermal effect of aerogel material for steel ladle insulation layer, Coatings 11 (2021) 1205, http://dx.doi.org/10.3390/coatings11101205.
[16] I. Mäkelä, V.V. Visuri, T. Fabritius, A mathematical model for the thermal state of a steel ladle, Ironmak. & Steelmaking: Process. Prod. Appl. 50 (2023) 867–877, http://dx.doi.org/10.1080/03019233.2023.2201544.

[17] K. Niu, W. Feng, A.N. Conejo, M.A. Ramirez-Argaez, H. Yan, 3D CFD model of ladle heat transfer with gas injection, Met. Mater. Trans. B 54 (2023) 2066–2079, http://dx.doi.org/10.1007/s11663-023-02816-2.
[18] H. Duan, C. Huang, L. Zhang, Numerical simulation of transient flow and heat transfer in a steel ladle during holding period, Met. Mater. Trans. B (2024) http://dx.doi.org/10.1007/s11663-024-03090-6.
[19] M. He, L. Wang, Y. Li, L. Zhao, Zhouhua Jiang, Qiang Wang, A model to predict coil temperature evolution during the whole thermal cycle process of ladle with a novel steel teeming technology, J. Therm. Sci. Technol. 17 (2022) http://dx.doi.org/10.1299/jtst.22-00259, 22-00259.
[20] W. Shaoyang, Q. Xin, Q. Dabin, L. Xudong, Z. Ling, Y. Jiegang, Study on the properties of periclase-forsterite lightweight heat-insulatingrefractories for ladle permanent layer, Ceram. Int. 48 (2022) 20275–20284, http://dx.doi.org/10.1016/j.ceramint.2022.03.308.
[21] F. Berntsson, P. Wikström, Thermal tracking of a ladle during production cycles, Int. J. Comput. Methods Eng. Sci. Mech. 24 (2023) 406–416, http://dx.doi.org/10.1080/15502287.2023.2253255.
[22] Surface-to-surface radiation model, Available at: https://doc.comsol.com/5.5/doc/com.comsol.help.heat/heat_ug_ht_features.09.044.html.
[23] Emissivity of specific materials. Cole-parmer, Available at: https://www.coleparmer.com/tech-article/emissivity-of-specific-materials.
[24] B. Glaser, M. Gornerup, D. Sichen, Thermal modelling of the ladle preheating process, Steel Res. Int. 82 (2011) 1425–1434, http://dx.doi.org/10.1002/srin.201100198.
[25] L. Jonsson, P. Jonsson, Modeling of fluid flow condition around the slag/metal interface in a gas stirred ladle, ISIJ Int. 36 (1996) 1127–1134, http://dx.doi.org/10.2355/isijinternational.36.1127.
[26] The Making, Shaping and Treating of Steel. Steelmaking and Refining Volume. 1998, The AISE Steel Foundation, ISBN: 0-930767-02-0, Chapter 11.
[27] E.T. Turkdogan, Fundamentals of Steelmaking, Maney Publishing, Leeds, 2010, p. 247.
[28] Isothermal domain, Available at: https://doc.comsol.com/5.5/doc/com.comsol.help.heat/heat_ug_ht_features.09.018.html.
[29] KANTHAL. Ladle preheating. Available at: https://www.kanthal.com/en/industries/steel/ladle-preheating/.